Journal of Ceramic Processing Research. Vol. 9, No. 3, pp. 317~320 (2008)

J O U R N A L O F
Ceramic Processing Research

Residual stress determination in plasma sprayed Al_2O_3 coatings

Jia Zhang[a], Huang Chen[a], Tohru Sekino[b], Seung Ho Kim[b] and Soo Wohn Lee[a,*]
[a]*Department of Materials Engineering, Sun Moon University, Asan, Chungnam 336-708, Korea*
[b]*The Institute of Scientific and Industrial Research, Osaka University, Osaka 567-0047, Japan*

Residual stress is a problem which could reduce the lifetime of plasma sprayed coatings. So it is necessary to find the relationship between plasma spray parameters and residual stress. In this study, a plasma spraying technique was used to deposit Al_2O_3 coatings on stainless steel substrates under different spraying parameters. The residual stresses were determined by an X-ray diffraction method. Furthermore, surface roughness and porosity of the plasma sprayed Al_2O_3 coatings were measured.

Key words: Plasma sprayed coating, X-ray diffraction, Spray power, Coating thickness, Residual stress.

Introduction

Plasma spray process can be used to deposit a wide range of materials, and plasma sprayed ceramic coatings have been widely used in many fields such as the nuclear, electronic, agriculture, steel casting etc. This technique is mostly utilized to produce coatings on structural materials. Such coatings provide protection against high temperatures, corrosion, erosion, wear; they can also change the appearance, and electrical properties of the surface. However, the residual stress which can arise in materials in almost every step of process [1], becomes a problem in plasma sprayed coatings when its magnitude exceeds the adhesive or cohesive strength of the coating, such that the coating fails, by debonding from the substrate, spalling or cracking [2]. An X-ray diffraction method was used to determine residual stress in this study.

Experimental Procedure

Nano-sized alumina (Al_2O_3) and titania (TiO_2) powders supplied by Hunan Biasfree Corp. (*China*), with mean diameters of 70 nm and 80 nm, respectively, were selected as the raw feedstock. The nano-sized Al_2O_3 and TiO_2 powders were reconstituted into micro-sized granules with a composition equivalent to the conventional Al_2O_3-3 wt%TiO_2 powder by spray-drying process. The aggregated powder obtained was subsequently sintered at medium temperature (800 °C) in a furnace in order to get a powder with more density. The morphologies for both the aggregated nanostructured Al_2O_3-3wt%TiO_2 powder and conventional Al_2O_3-3wt.%TiO_2 powder are shown in Fig. 1. The spray-dried nanostructured powders are spherical with sizes in the range of 10-30 μm Fig. 1(a), while, the conventional powder exhibits an angular and irregular morphology with sizes from 20 to 50 μm Fig. 1(b).

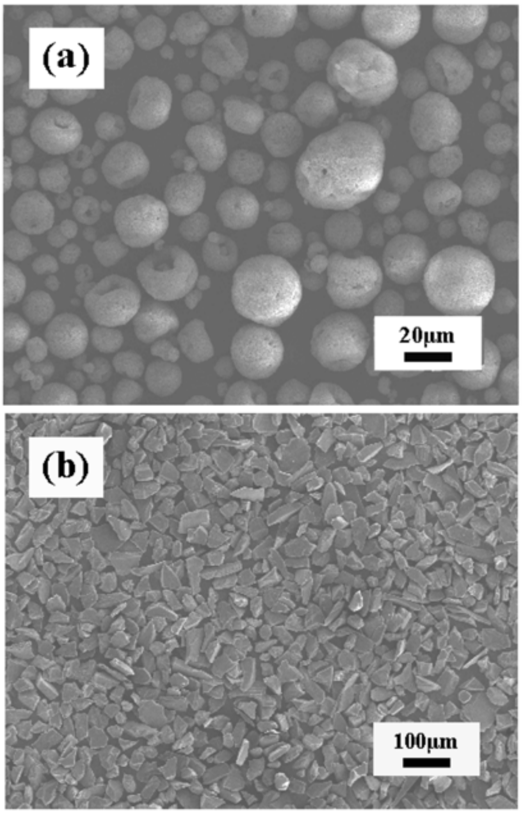

Fig. 1. SEM morphologies of Al_2O_3-3 wt%TiO_2 powders: (a) nanostructured and (b) conventional.

Figure 2 shows their XRD patterns. The trigonal α-Al_2O_3 appeared in the nanostructured and conventional powders. In additional, a small amount of rutile phase of TiO_2 was found in the nanostructured powder. However, only Ti_3O_5 appeared in the conventional Al_2O_3-3 wt%TiO_2 powder, which was formed during the fusing and crushing process.

*Corresponding author:
Tel : +82-41-530-2364
Fax: +82-41-543-2798
E-mail: swlee@sunmoon.ac.kr

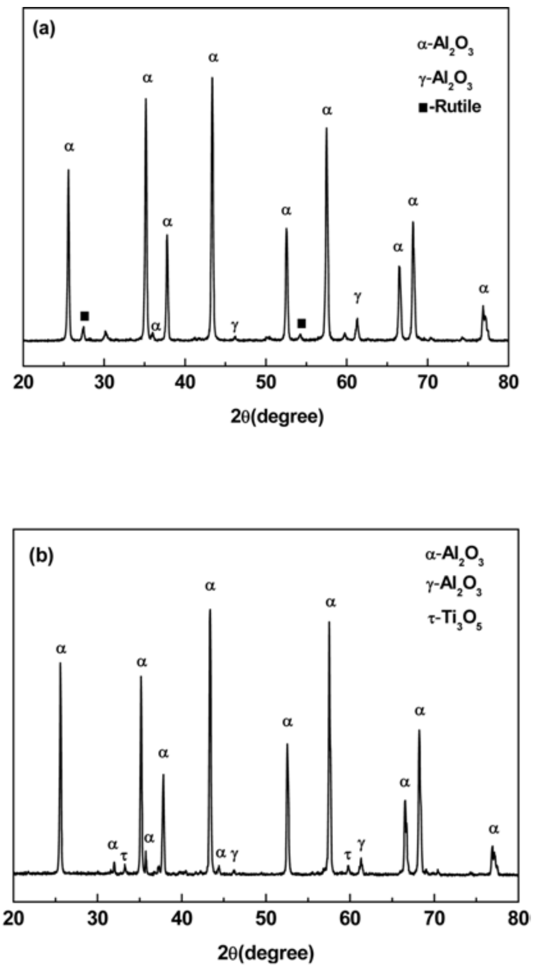

Fig. 2. XRD patterns of Al_2O_3-3 wt% TiO_2 powders: (a) nanostructured and (b) conventional.

Plasma spraying was carried out in an A-2000 atmospheric plasma spraying equipment with a F4-MB gun (*Sulzer Metco AG, Switzerland*) which is mounted on an ABB robot (*ABB, Sweden*). The feedstock was fed with a Twin-System 10-V feeder (*Plasma-Technik AG, Switzerland*). For each powder, four types coatings were deposited under different deposition parameters as listed in Table 1. H_2 and Ar were used as the plasma gases. The AISI 304 stainless steel plates with dimensions of 50 × 20 × 2 mm^3 were used as the substrates. Before the plasma spraying, all the stainless steel plates were degreased ultrasonically in acetone and grit-blasted with 220 grit alumina.

The X-ray source was a Cr tube, Ni and Fe were used as the filters, in order to get a CrKα beam (2.2897 Å) to achieve as large a peak shift $\Delta\theta$ as possible. The X-ray diffraction from these coatings, boosted the tilt angle ψ from 0-45° in 5° steps. A position sensitive proportional counter (PSPC, Rigaku Co.,Ltd., Japan) was used to record and analyse the X-ray diffraction beams. The recorded peaks were stored in a computer for analysis.

Table 1. Deposition parameters for spraying nanostructured Al_2O_3 coatings

Samples	Parameters	a	b	c	d
N-Al_2O_3	Spray distance (mm)	80	100	110	120
	Spray power (kW)	33.0	43.5	43.2	47.5
C-Al_2O_3	Spray distance (mm)	80	100	110	120
	Spray power (kW)	33.5	43.5	43.2	48.2

The peak top method, the FWHM (full wave at half maximum) method and the Gravity method were used to calculate residual stresses. The peak top method uses the maximum intensity of diffraction peaks, the FWHM method use the half maximum intensity of diffraction peaks, the Gravity method use all the information of the peaks and get a average value [3].

Surface roughness (Ra) measurement of the plasma sprayed coatings was conducted with a 0.5 mm/s traverse speed over 3.2 mm length using a roughness tester (Form Talysurf Plus, Rank Taylor Hobson Limited, England, UK). The reported values come from the mean of three tests for each sample.

Porosity measurements were evaluated by image analysis. The evaluation steps are: (1) take SEM images on cross-sections of the plasma sprayed Al_2O_3 coatings at a magnification of × 1000, (2) enhance the image, to eliminate all interferences and clearly identify the pores; (3) extract the pores from the background; (4) calculate the area fraction of the pores on the image [4].

Results and Discussion

Figures 3 and 4 present the SEM morphologies of the plasma sprayed nanostructured and conventional Al_2O_3 coatings deposited under different conditions, respectively. From these micrographs, their thicknesses were calculated. Tables 2 and 3 present the properties of these coatings. Judging from their thickness and spray cycles, it is clear that their deposition efficiencies are quite different and can be correlated to their spraying conditions, namely

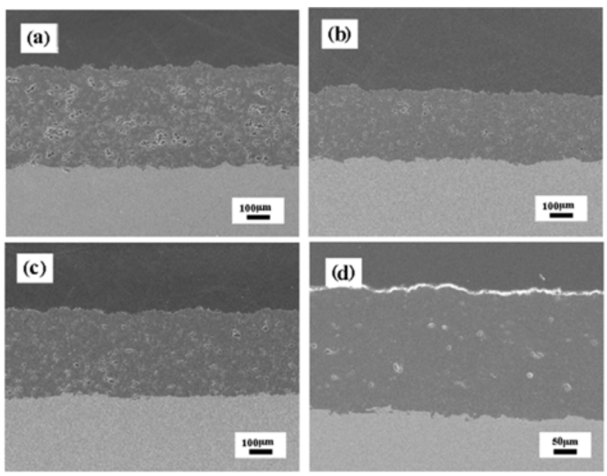

Fig. 3. SEM morphologies of the plasma sprayed nanostructured Al_2O_3 coatings deposited under different conditions: (a) N-Al_2O_3-a, (b) N-Al_2O_3-b, (c) N-Al_2O_3-c, (d) N-Al_2O_3-d (See Table 1).

Table 2. Residual stress of nanostructured Al_2O_3 coatings

Samples		Residual stress (MPa) + : tensile, − : compressive					
		FWHM		Gravity		Peak Top	
		Avg.	SD	Avg.	SD	Avg.	SD
N-Al_2O_3	a	−65.66	50.79	−127.32	92.88	−198.39	86.65
	b	−185.83	93.57	−137.10	59.43	−156.77	86.33
	c	−153.92	102.18	−70.80	93.87	−91.65	87.63
	d	−301.78	92.24	−367.97	94.80	−362.14	173.23
C-Al_2O_3	a	41.68	169.15	94.06	102.98	−33.01	268.53
	b	155.75	184.67	116.50	145.09	243.87	241.07
	c	503.90	185.00	416.45	180.32	375.60	316.35
	d	−258.85	244.93	−236.41	306.83	−533.71	301.41

spraying power and spraying distance. With an increase of the spraying power and spraying distance, the deposition efficiencies for the plasma sprayed conventional Al_2O_3 powder were increased. The highest deposition efficiency was achieved at a spraying power of 48.2 kW and a spraying distance of 120 mm. In the case of the aggregated nanostructured Al_2O_3 powder, within the scope of the investigated spraying parameters, no significant linear relationship was observed. Instead, under a lower spraying power and with a shorter spraying distance, the aggregated nanostructured Al_2O_3 powder presented higher deposition efficiency than the conventional Al_2O_3 powder. Conversely, it is lower. This could be ascribed to the very fine powders in the aggregated nanostructured Al_2O_3 powder being evaporated under the higher spraying power during the plasma spraying. The spraying parameters have a strong influence on their porosities. Larger pores (about or larger than 5 μm) were observed for plasma sprayed Al_2O_3 coatings deposited under the lowest spraying power (33.5 kW). These larger pores resulted from a lower melting degree of the feedstock as evidenced by the unmelted particles in the pores. From Table 3, no clear

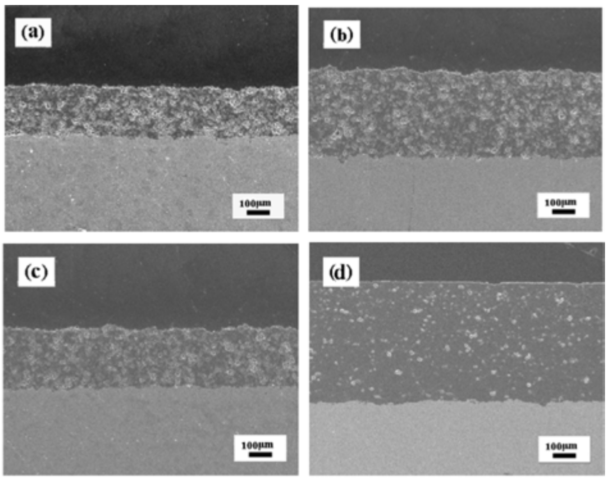

Fig. 4. SEM morphologies of the plasma sprayed conventional Al_2O_3 coatings deposited under different conditions: (a) C-Al_2O_3-a, (b) C-Al_2O_3-b, (c) C-Al_2O_3-c, (d) C-Al_2O_3-d(See Table 1).

Table 3. Properties of the plasma sprayed nanostructured Al_2O_3 coatings

Samples		Thickness (μm)	Roughness (μm)	Porosity (%)
N-Al_2O_3	a	420	2.47 ± 0.04	25.0 ± 3.0
	b	300	2.18 ± 0.05	8.0 ± 1.2
	c	360	2.06 ± 0.06	10.0 ± 1.6
	d	260	2.06 ± 0.07	2.0 ± 0.4
C-Al_2O_3	a	210	1.82 ± 0.06	37.0 ± 5.0
	b	360	2.10 ± 0.10	29.0 ± 3.0
	c	240	2.10 ± 0.10	18.0 ± 3.0
	d	480	2.27 ± 0.01	5.0 ± 1.0

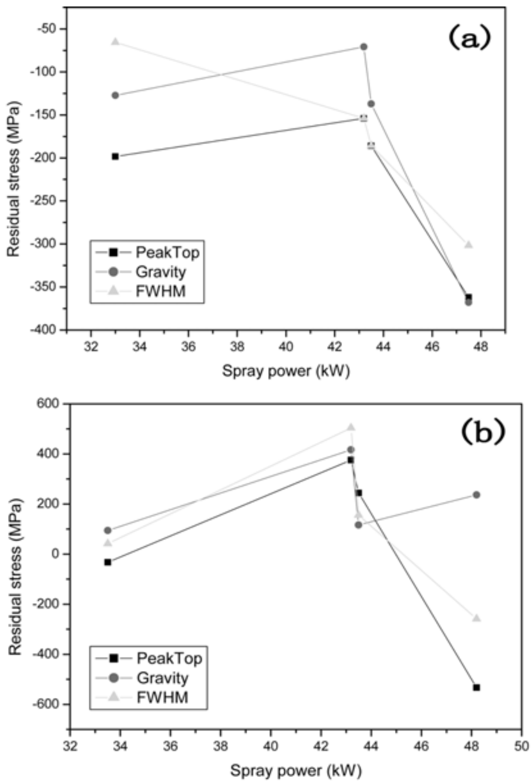

Fig. 5. Variation of residual stress with the spray power in the plasma sprayed nanostructured Al_2O_3 (a) and conventional Al_2O_3 coatings (b).

relationship between the surface roughness and the spraying conditions was found in this study. It seems that the spraying conditions investigated have little influence on both the plasma sprayed nanostructured and conventional Al_2O_3 coatings.

From Fig. 5, it is noted that there is a critical spray power for the plasma sprayed nanostructured and conventional Al_2O_3 coatings. But the behaviors of the residual stress for the different coatings are not the same. For the nanostructured Al_2O_3 coatings, the residual stresses are compressive, the residual stress increases when the spray power exceeds the critical power. 43 kW is the optimal spray power which made the residual stress become the lowest.

For the conventional Al_2O_3 coatings, the residual stresses are tensile when the spray power is no more than 43.5 kW. At 33.5 kW spray power, the lowest residual stress for the conventional Al_2O_3 coating was achieved. It is ascribed to its higher porosity as listed in Table 3. When the spray power increased from 33.5 kW to 43.2 kW, the residual stress increased. For all the coatings, the values of the maximum tensile stresses appear at the spray power of 43.2 kW as plotted in Fig. 5(b) Under the highest spray power (48.2 kW), the residual stresses are compressive except for the value obtained from the gravity method.

Residual stresses, originating from the large temperature differences, are commonly divided into quenching and thermal stresses. The quenching stress is a result of rapid quenching of the molten droplet upon impact on the substrate. As its temperature drops, its contraction is restricted by the underlying substrate, therefore, tensile stress develops in the layer. Tensile stresses at the surface of the coatings are mainly due to the rapid quenching of the plasma sprayed droplets arriving at the substrate and to the surface of the coating in the growth process which is at a lower temperature than the molten sprayed particles. A lower tensile stress at the surface due to the typical growth of the coatings and quenching effects is observed. The in-plane compression stress state is related to an increase in the elastic modulus of the material due to the sintering effects such as homogeneity of the pores and reduction in the width of cracks. After thermal cycling, the state of tensile stress also increases but reaches lower values than for the annealed samples. This difference can be explained by some micro-cracks within the coatings that have an opposite effect to the sintering process developed during the exposure at high temperature.

At the instant the first splat of the coating impinges upon the substrate, the stress in the coating is tensile, while that in the substrate is compressive. The contraction related to the cooling of the molten splat is restricted to some extent by the substrate. The first coating splat impinging upon the substrate surface is the most critical because the substrate is locally heated up from a low temperature by the splat and the splat is cooled suddenly due to the fast heat dissipation, leading to the abrupt stress and strain changes. As a new deposit layer is deposited, its contraction during rapid cooling is restricted by adherence to the substrate. Subsequent layers experience a similar process, through equilibration of forces, the underlying material's stress shifts towards compression. This leads to a stress gradient with more tensile stress on the surface, whose magnitude is limited by the deposit strength. This gradient creates a significant bending moment which can lead to deposit delamination when the deposit thickness reaches a critical point. The tensile stress in the deposit is balanced by compression in the substrate and is partially accommodated by substrate contraction and bending. If the forces and moments acting on the substrate reach a sufficient magnitude to cause yielding, plastic deformation occurs. After cooling down to room temperature, a higher compressive stress is developed within the coatings due to the differences between the coefficients of thermal expansion of the substrate and coating. Another factor which influences the residual stresses at the interface between the top coat and bond coat is the growth of the thermal growth oxide developed at high temperatures. So, with an increase the coating thickness, the larger residual stresses were obtained in the coatings. The interlayer bonding can make the residual stress decrease.

Conclusions

There is a critical spray power for the plasma sprayed nanostructured and conventional Al_2O_3 coatings. For nanostructured Al_2O_3 coatings, 4 3kW is the optimal spray power. For conventional Al_2O_3 coatings, a spray power of 33 kW can be used to deposit Al_2O_3 coatings with lower residual stress.

Acknowledgements

The authors would like to thank the financial support from the ITEP Grant (10027929-2006-1).

References

1. C.C. Berndt, Thermal Spray Technology, ASM Handbook, ASM International (2004).
2. M.R. James and O. Buck, Quantitative Nondestructive Measurements of Residual Stresses, CRC, Critical Reviews in Solid State and Materials Sciences 9 (1980).
3. B.D. Cullity and S.R. Stock, Elements of X-ray Diffraction. Addison Wesley, Massachusetts (2001).
4. J.F. Li, H. Liao, X.Y. Wang, C. Coddet, H. Chen and C.X. Ding, Thin Solid Films 460 (2004) 101-105.